JACS
JOURNAL OF THE AMERICAN CHEMICAL SOCIETY
pubs.acs.org/JACS
Article

Mechanistic Investigation of a Photoredox Cycloaddition Chain Reaction

Annemarie A. Lee and John R. Swierk*

Cite This: J. Am. Chem. Soc. 2024, 146, 34900−34908
Read Online
ACCESS | Metrics & More | Article Recommendations | Supporting Information

ABSTRACT: Photoredox catalysis is important in modern organic chemistry and the development of new synthetic methods. Mechanistic insights, particularly with photoredox chain reactions, are underdeveloped. This study combines quantum yield (QY) measurements, transient absorption spectroscopy (TAS), and electrochemical analysis to rigorously characterize the mechanism and rate constants of a ruthenium-catalyzed photoredox chain [4 + 2] cyclization between *trans*-anethole and isoprene. TAS and steady-state photochemical measurements (QY studies) reveal the role of oxygen in chain propagation as a secondary electron acceptor. The key kinetic competition between chain propagation and termination is identified by TAS and explored with kinetic modeling.

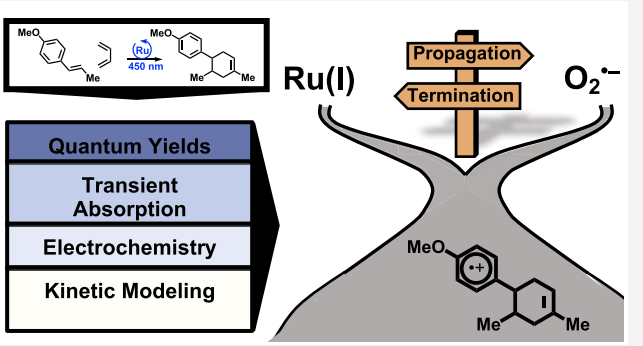

INTRODUCTION

The application of visible light photochemistry to small molecule synthesis (photoredox) is steadily growing in popularity. In 2008 and 2009, work by MacMillan, Yoon, and Stephenson triggered a renaissance in the application of light to organic synthesis.[1−3] Many photoredox reactions rely on visible light to excite a photocatalyst, often a transition metal complex incorporating ruthenium or iridium, with long-lived excited states.[5−8] They also offer the ability to absorb light at wavelengths that many organic small molecules will not, allowing for selective excitation. Upon excitation, the photocatalyst acts as a potent oxidant or reductant and produces intermediates that can be leveraged in important transformations that are not as accessible through classical synthetic methods.[5] More specifically, following excitation, photoredox reactions proceed through a single electron transfer (SET)[9] to produce a radical ion, which is able to participate in radical chemistry. In general, the use of excited states allows for the replacement of potentially harsh reaction conditions with visible light.

Though it is a key aspect of photoredox catalysis, the efficiency of light utilization is rarely a primary consideration. Efficient light utilization becomes critical when laboratory-scale demonstrations are transferred to larger-scale agricultural or pharmaceutical applications.[10−12] One way to measure photon utilization in chemical reactions is through the reaction quantum yields (QY).[13] Strictly speaking, IUPAC defines "quantum yield" as moles of product divided by incident photons produced from a monochromatic light source, while "quantum efficiency" is defined as moles of product divided by moles of absorbed photons from a broadband light source. The term "photonic efficiency" is recommended for a measure of moles of product divided by moles of incident photons. Because "quantum efficiency" and "photonic efficiency" are not in wide usage, we have instead classified QY in two ways: the moles of product divided by incident photons (external quantum yield) or the moles of product divided by photons that were absorbed (internal quantum yields).[14] The QY can be tracked over time and offers valuable mechanistic information and kinetic insights.

We recently demonstrated that high QY reactions are attractive for scaling photoredox reactions to industrial settings.[11] The use of photochemical chain reactions, which produce multiple product molecules from a single photon, is one way to achieve high QY reactions. Bodenstein was one of the first to take an interest in photochemical chain reactions after noticing that some chemical processes produced an output exceeding what was expected based on the units of light invested.[15] Even before 2008, a few studies observed reactions that displayed a chain behavior. Ledwith and co-workers published a study on the mechanisms of photoredox catalysis involving the [2 + 2] cycloaddition of *N*-vinyl carbazole. Their work revealed a novel chain reaction proceeding through cationic cyclobutane with fluorenone or chloranil photo-

Received: October 13, 2024
Revised: November 24, 2024
Accepted: November 26, 2024
Published: December 9, 2024

https://doi.org/10.1021/jacs.4c14255
J. Am. Chem. Soc. 2024, 146, 34900−34908

Scheme 1. Diels-Alder [4 + 2] Reaction Scheme between *trans*-Anethole and Isoprene

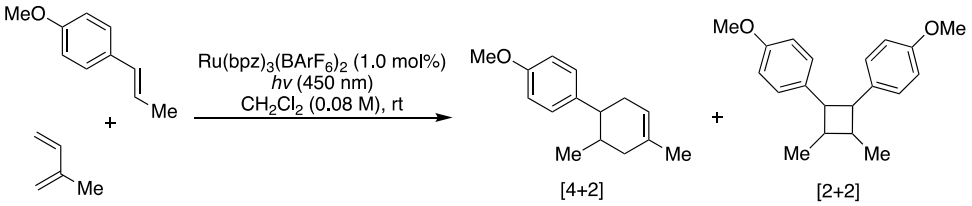

sensitizers.[16] Additionally, Freeman and Schulte led a study on the 1,3-cyclohexadiene dimerization where the reaction proceeded via a chain reaction mechanism.[17]

More recently, several studies have focused on visible light photocatalytic reactions that were found to exhibit chain behavior in a diverse array of synthetic applications. One example is the aldehyde alkylation with bromomalonate that was originally proposed in a dual catalytic system by Nicewicz and MacMillan and further mechanistically investigated by Cismesia and Yoon.[3,18] Another reaction demonstrating chain behavior is the Michael addition reaction that Glorius and co-workers proposed to work through a combination of hole catalysis and transition metal photocatalysis.[19] Cyclization reactions, such as the [3 + 2] and [4 + 2] cycloaddition reactions, have also been identified as chain reactions.[1,20] In addition to these, experimental spectroscopic and kinetic simulations were carried out to study chain behavior in the polymerization of methyl acrylate at room temperature.[21]

While chain reactions involving neutral radicals are well established,[22−24] chain reactions involving radical ions are not as well understood. The latter is particularly relevant as photoredox chain reactions involve photoinduced electron transfer to produce a radical ion. Chabuka and Alabugin outlined the electrochemical and thermodynamic guidelines for constructing radical ion chain reactions using a hole-catalyzed Diels−Alder reaction as a model reaction.[25] Specifically, they pointed out that the product radical ion should be more oxidizing than the starting material if chain behavior is to be observed. They describe the process as hole upconversion, and though their focus was not on photoredox chain reactions, the underlying principles should be the same in a photochemical context.

Mechanistic studies of photoredox reactions are still relatively rare.[26] Most mechanistic and kinetic studies have focused on nonchain photoredox reactions,[4,14,20,26−34] though there is a small subset of these reports focused on photoredox chain reaction mechanisms. DiRocco, Knowles, and co-workers applied a combination of electrochemical, kinetic, and spectroscopic studies to identify the chain reactions in the photocatalytic dehydrogenation of indoline. Isotope effects were used to confirm the presence of the chain behavior.[35] Damrauer and co-workers also combined DFT calculations with experimental quenching to study the propagation pathway in a phenothiozine photocatalyzed polymerization.[36] Chen, Zheng, and co-workers examined the propagation pathway in a [3 + 2] cyclization reaction through the use of mass spectroscopy.[37] Orr-Ewing investigated chain behavior in polymerization reactions through a series of ultrafast laser spectroscopy studies.[38] Glorius and co-workers applied both experimental and computational studies to determine how chain propagation influences the chemo- and regioselectivity of the C−O and C−C bonds that are forming.[19]

In 2011, Yoon and co-workers demonstrated a photoredox [4 + 2] Diels−Alder reaction cycloaddition involving electron-rich dienophiles (Scheme 1).[18] The study demonstrated a successful cyclization through photoredox catalysis and exhibited an impressive substrate scope, specifically electron-rich dienophiles that are difficult to cyclize under mild conditions. Cismesia and Yoon later showed that the cyclization proceeded via a chain reaction using the photoredox cycloaddition of anethole and isoprene as a model reaction.[1] Though the diene−dienophile pair are both electron-rich, which makes the pairing electronically unfavorable under thermal conditions, a photoredox radical ion route enables cycloaddition to occur. Furthermore, they were able to develop a method for carrying out Diels−Alder cycloadditions that uses low catalyst loading and is conducted with visible light, making it a much more practical method of synthesis.[1] Yoon's proposed mechanism begins with the excitation of the ruthenium catalyst to an excited triplet state, which then oxidizes the dienophile (anethole) to generate a Ru(I) species and the anethole radical cation. The radical cation then cyclizes with isoprene to generate the [4 + 2] product radical cation, $[4 + 2]^{\bullet+}$. At this stage, the mechanistic proposal is that the reaction can continue in one of two ways: (1) $[4 + 2]^{\bullet+}$ can either be reduced by Ru(I) to become the product via a closed cycle pathway or (2) $[4 + 2]^{\bullet+}$ can proceed via a propagation pathway, where a new molecule of anethole is oxidized to produce the final product and a new anethole radical cation intermediate. Previous QY measurements observed a QY of 41 in the presence of oxygen, suggesting a chain propagation length of 41. An unproductive [2 + 2] cyclization between the anethole radical cation and another molecule of anethole is also possible.

Despite the recognition of photoredox chain reactions, there is a significant gap in our understanding of how to intentionally design chain reactions. Specifically, the kinetic and mechanistic principles necessary for long-chain, high QY reactions are not well understood. Using the [4 + 2] cycloaddition first demonstrated by Yoon and colleagues as a model for photoredox chain reactivity, this study demonstrates a comprehensive mechanistic and kinetic analysis of a photoredox chain reaction. A combination of QY measurements, electrochemistry, transient absorption spectroscopy (TAS), and kinetic modeling is used to determine rate constants for individual reaction steps, which are then connected with overall performance. The data demonstrate that for chain reactions, the key kinetic competition is between the propagation step and reduction of product radical cation by the reduced photocatalyst and highlight the important role of secondary electron acceptors in slowing down the $[4 + 2]^{\bullet+}$ reduction step.

https://doi.org/10.1021/jacs.4c14255
J. Am. Chem. Soc. 2024, 146, 34900−34908

METHODS

Ruthenium(III) chloride, 2,2-bipyrazine, sodium tetrakis [3,5-bis-(trifluoromethyl)phenyl]borate, *trans*-anethole, isoprene, and dibromomethane were purchased from Sigma-Aldrich. Dichloromethane (DCM) was purchased from Fisher Scientific. 9-Mesityl-3,6-di-*tert*-butyl-10-phenylacridinium tetrafluoroborate (MesAcr) was purchased from Millipore-Sigma. All reagents were used as received unless stated otherwise. Tris(2,2′-bipyriazyl)ruthenium(II) Bis(tetrakis(3,5-bis-(trifluoromethyl)phenyl)borate), $[Ru(bpz)_3]^{2+}$, was synthesized as previously described in the literature.[39]

Quantum Yield (QY) Measurements. The external QY was determined using a modification of Yoon's reaction conditions and applying the QY measurement method described in our previous reports.[1,4,14] The $[Ru(bpz)_3]^{2+}$ photocatalyst (1.6 μmol, 1.0 mol %), *trans*-anethole (0.16 mmol, 1 equiv), and isoprene (1.6 mmol, 10 equiv) were added to a 1 cm path length cuvette. If the reaction was run under an inert atmosphere, the solvent DCM (2 mL) was purged for 45 min before being added to the cuvette with a syringe. Otherwise, the DCM was added directly to the cuvette without purging. The reaction mixture was set 30 cm away from and allowed to stir in front of a 450 nm LED light source (Thorlabs M450LP2) with a stir bar. QY measurements were taken under varying conditions, including open to air and under an inert atmosphere. An additional condition, a pure O_2 atmosphere, was also examined by purging the solvent with pure O_2 for 30 min before addition to the cuvette via syringe. The reactions were exposed to light for a specified amount of time (1−2.5 h) at a power of 100 μW cm^{-2}. The LED light calibration was measured with a photodiode (Thor Laboratories S120C). The concentration of O_2 in DCM under an air atmosphere (0.2 atm P_{O2}) was determined to be 1.88 and 9 mM under a pure O_2 atmosphere using the Henry's Law constant.[40]

The product yield as a function of reaction time was determined using quantitative NMR (Table S3 and Figures S1−S9). Following sample collection, dibromomethane was added as an internal standard to quantify the product. A small sample of the reaction mixture (25 μL) was dissolved in chloroform-*d*, and the ^{1}H NMR spectrum was obtained with a Bruker 400 MHz NMR. The external QY was calculated via the equation below.

$$\text{quantum yield} = \frac{\text{moles of product}}{\text{moles of incident photons}}$$

Transient Absorption Spectroscopy (TAS) Experiments. TAS experiments were conducted with a Spectra-Physics Quanta-Ray Pro-290 pulsed Nd:YAG laser paired with a PrimoScan OPO (optical parametric oscillator).[14] An excitation wavelength of 430 nm was used for all of the TAS experiments. The laser was set to maintain an output power of 2.8 W before the OPO and a power density at the sample of 20.2 mW/cm^2. Transient spectra were collected with an Andor Kymera Spectrograph and Andor iStar CCD (charge-coupled device) camera. Single-wavelength data was collected using a custom setup.[14] Data was collected from probe wavelengths of 300−800 nm, with a pump wavelength of 430 nm. Time delays of 100 ns to 10 μs were used.

TAS samples contained $[Ru(bpz)_3]^{2+}$ (27 μM), 53 mM anethole, and 0.50 M isoprene dissolved in DCM. Samples were changed after about 15 min due to the formation of the product with laser exposure. Data for the single-wavelength experiments was collected in 6.4 ns intervals up to 12 μs and then continued in 1 μs intervals up to 10 ms. For the short-time data traces, data was also collected with the probe blocked. The data collected with the probe blocked was then subtracted from the TAS data to remove any residual laser scattering or emission. Single-wavelength traces were collected at 6−9 different wavelengths ranging from 370 to 610 nm for each condition. Samples were changed with every wavelength observed. A detailed kinetic model was fit to the experimental TAS traces to determine the rate constants (Supporting Information).

Spectroelectrical Studies. Spectroelectrochemical experiments were all performed with a BioLogic SP-50 potentiostat, platinum counter electrode (Pine), gold working electrode (Pine), and a 1 cm path length electrochemical cell that could be purged with Ar gas. All electrochemical potentials were applied in reference to a Ag/AgCl reference electrode, while all samples were prepared in a 0.1 M ammonium hexafluorophosphate (NH_4PF_6) supporting electrolyte solution. Spectra were collected with a Shimadzu UV-2600 UV−vis spectrophotometer. Because the anethole radical cation did not produce a stable spectroelectrochemical spectrum, the difference spectrum was obtained through TAS using a photocatalyst, MesAcr, which could be subtracted out of the transient spectrum to obtain the spectrum for the known anethole radical cation intermediate (Figure S13).[34] The spectrum of the MesAcr radical ion was obtained using the same spectroelectrochemical method described above (Figure S14).

RESULTS AND DISCUSSION

Photochemical Studies. Under steady-state illumination, successful cycloaddition was observed with product yields comparable to those reported by Yoon et al. (Figure S15).[1] We observed a maximum QY of 43 for the [4 + 2] cyclization reaction between anethole and isoprene when open to air (Figure 1), which is consistent with the QY of 41 measured by Yoon. A QY greater than 1 is also consistent with a chain reaction.

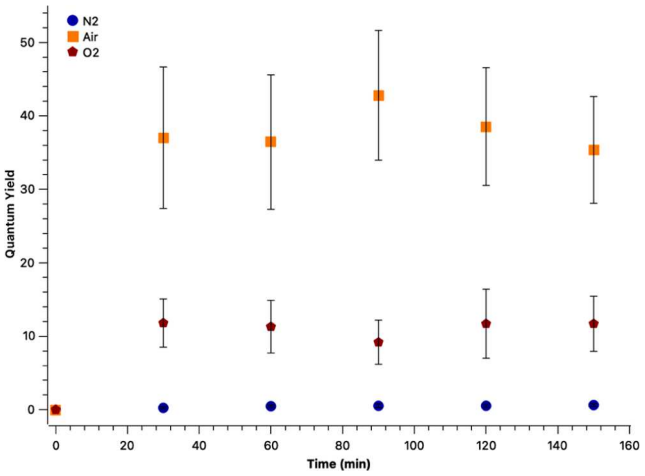

Figure 1. External QY of the reaction while irradiated by a 450 nm LED (100 μW cm^{-2}) when open to air (orange) and purged with N_2 (blue) and O_2 (red).[4]

Under an inert atmosphere, the QY for the cyclization reaction reached a maximum of 1.79. The decrease in QY indicated a significantly lower number of propagation cycles per photon and suggested that oxygen plays a role in enabling more efficient chain reactions. To further explore the role of oxygen, the reaction mixture was purged with 100% oxygen gas. However, the maximum QY was 11.8. While the QY of 11.8 indicates more chain propagations than under inert conditions, the QY is lower compared to reactions run in ambient air. This is likely due to triplet−triplet energy transfer and deactivation of the ruthenium catalyst's excited state, effectively wasting the absorbed photons.[41−43]

We also observed that the product distribution exhibited a dependence on the concentration of isoprene. When the concentration of isoprene was kept at the original three equivalents used in Yoon's report,[1] we observed a 14.1% product yield of the [2 + 2] cyclization side product and less of the [4 + 2] product. In comparison, using 10 equiv of isoprene

https://doi.org/10.1021/jacs.4c14255
J. Am. Chem. Soc. 2024, 146, 34900−34908

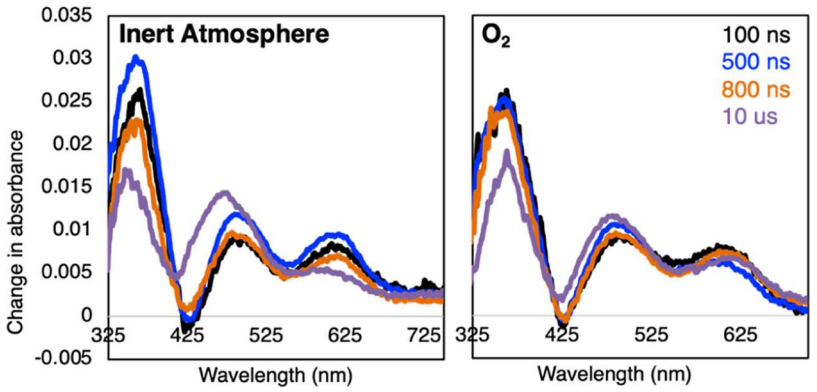

Figure 2. Transient absorption spectra showing the changes in absorbance measured at the specified delay times after 450 nm excitation of 27 μM $[Ru(bpz)_3]^{2+}$, 53 mM anethole, and 0.5 M isoprene. Samples were tested under an inert atmosphere (left) and when open to air (right).

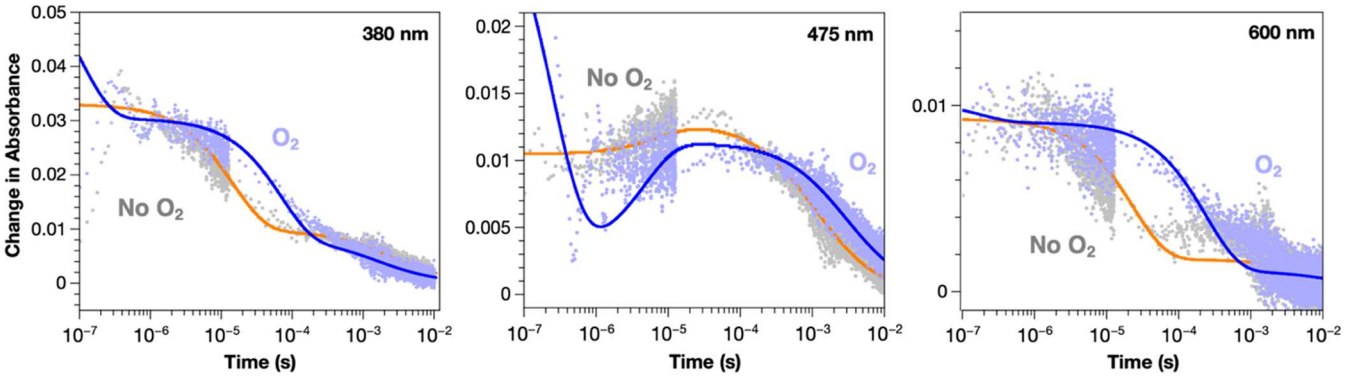

Figure 3. Single-wavelength traces for 27 μM $Ru(bpz)_3$ and 53 mM anethole at 380, 475, and 600 nm under an inert atmosphere (gray) and in the presence of oxygen (violet). The orange and blue solid lines represent the kinetic model fit to the experimental data. The solid orange line is fit to data under an inert atmosphere, while the solid blue line is fit to data in the presence of oxygen.

led to a reaction with a product yield of only 3.6% [2 + 2] product (Figure S16).

With these results, we hypothesized that in the presence of oxygen, an electron might be transferred from the reduced Ru(I) photocatalyst to oxygen and generate superoxide. This in turn might lead to a slower reduction of $[4 + 2]^{\bullet+}$ and make propagation via reduction of $[4 + 2]^{\bullet+}$ by another anethole molecule more competitive. To further explore this hypothesis, we utilized transient absorption spectroscopy.

Transient Absorption Spectroscopy (TAS). Figure 2 shows the transient spectra from 100 ns to 10 μs for $[Ru(bpz)_3]^{2+}$, *trans*-anethole, and isoprene. Transient spectra were also collected for samples with $[Ru(bpz)_3]^{2+}$ and anethole (Figure S17). The spectra display transient absorption features centered around 365, 495, and 610 nm, with a small bleach centered around 430 nm. Spectroelectrochemical experiments were instrumental in interpreting these features. The bleach at 430 nm was assigned to the formation of Ru(I) (Figure S18) by spectroelectrochemistry, which is consistent with other spectroelectrochemical studies of $[Ru(bpz)_3]^{2+}$,[44] though the bleach for the Ru(I) species was not as apparent in the TAS spectrum as expected. After examining the difference spectra for the radical cations of [4 + 2] and [2 + 2] cycloaddition products, it was concluded that absorption features from these species were masking some of the Ru(I) bleach, particularly in the region of 400−550 nm where both product radical cation species have strong absorption bands (Figures S19 and S20). Specifically, the peak centered around 495 nm was assigned to overlapping $[2 + 2]^{\bullet+}$ and $[4 + 2]^{\bullet+}$ intermediates. Due to the instability of the anethole radical cation under electrochemical conditions, the difference spectrum for the anethole radical cation was generated using TAS. The difference spectrum revealed strong peaks at 610 and 365 nm that were also assigned to the anethole radical cation by Nicewicz.[34] Taken together, this suggests that anethole oxidation is rapid and that a significant fraction of the anethole radical cation undergoes cyclization within the first 100 ns.

After interpreting the features of the TAS spectra at 100 ns, our focus turned to understanding absorption changes as a function of time. Under an inert atmosphere, as the delay time was increased, the consumption of the anethole radical cation was observed through a decrease of intensity in the peaks at 365 and 610 nm (Figure 2). In contrast, the transient spectra in air showed minimal change in the signals related to the anethole radical cation even at 10 μs. As demonstrated by the QY, when under ambient air, the reaction exhibits chain behavior. We conclude that the persistence of the anethole intermediate at longer times in air is due to the propagation step replenishing the anethole radical cation. As the propagation step proceeds, with each product molecule that is made, a new molecule of anethole radical cation is formed. We suggest that this explains the persistent peak at 610 nm in the TAS spectra.

Before investigating individual pathways through single-wavelength TAS, we determined the initial concentrations of the reaction intermediates. Each intermediate's spectrum was converted to molar absorptivity and fit to the TAS spectra at 100 ns. The concentrations of each intermediate were varied

https://doi.org/10.1021/jacs.4c14255
J. Am. Chem. Soc. 2024, 146, 34900−34908

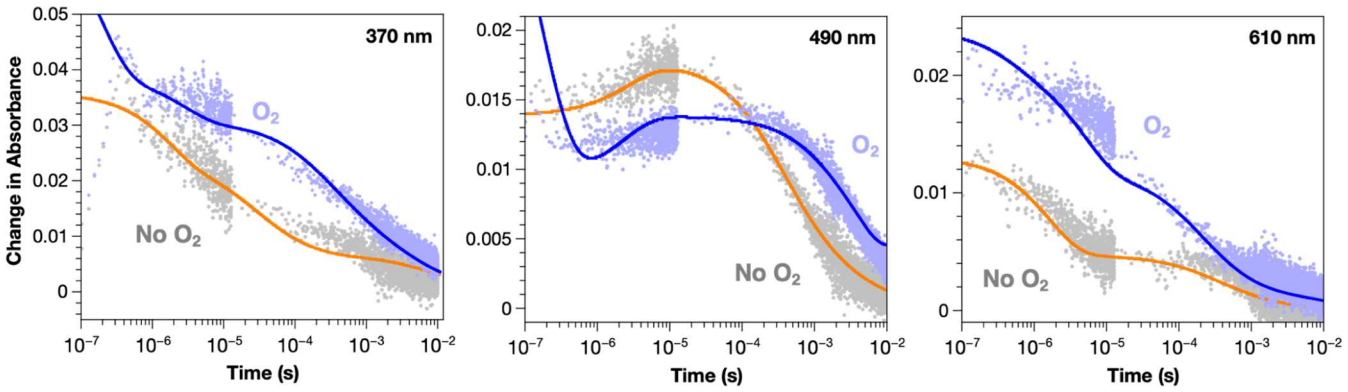

Figure 4. Single-wavelength traces for 27 μM $Ru(bpz)_3$, 53 mM anethole, and 0.5 M isoprene at 370, 490, and 610 nm under an inert atmosphere (gray) and in the presence of oxygen (violet). The orange and blue solid lines represent the kinetic model fit to the experimental data. The solid orange line is fit to data under an inert atmosphere, while the solid blue line is fit to data in the presence of oxygen.

until a good fit with the TAS spectra was obtained (Figures S21 and S22).

In order to probe the kinetics of individual reaction pathways, a series of steady-state emission quenching and TAS single-wavelength experiments were performed. The rate constant for emission quenching of $[Ru(bpz)_3]^{2+}$* by anethole (k_q) was determined as 1.1×10^{10} M^{-1} s^{-1} through emission quenching experiments and Stern–Volmer analysis. This value was consistent with the value of 1.4×10^9 M^{-1} s^{-1} reported by Yoon (Figure S23)[1] when considering that Yoon used a longer, 395 ns for $[Ru(bpz)_3]^{2+}$* instead of the 41 ns we measured by transient emission. Additionally, quenching of $[Ru(bpz)_3]^{2+}$* by the [2 + 2] and [4 + 2] products, ($k_{q[2+2]}$) and ($k_{q[4+2]}$) were also determined by Stern–Volmer analysis and found to be 5.87×10^9 and 2.28×10^9 M^{-1} s^{-1}, respectively (Figures S24 and S25). The value for quenching by the [2 + 2] product agreed well with the previously reported rate constant of 5.37×10^9 M^{-1} s^{-1} by Moore.[43]

Four different conditions were probed by TAS experiments in order to limit the number of parameters that were being determined in each experiment: (1) $[Ru(bpz)_3]^{2+}$ and anethole under an inert atmosphere; (2) $[Ru(bpz)_3]^{2+}$ and anethole under air; (3) $[Ru(bpz)_3]^{2+}$, anethole, and isoprene under an inert atmosphere; and (4) $[Ru(bpz)_3]^{2+}$, anethole, and isoprene under air. Figure 3 shows representative single-wavelength data for conditions 1 and 2 ($[Ru(bpz)_3]^{2+}$ and anethole), while Figure 4 shows representative single-wavelength data for conditions 3 and 4 ($[Ru(bpz)_3]^{2+}$, anethole and isoprene) under an inert atmosphere (gray dots) and air (violet dots). Consistent with the transient spectra, the single-wavelength data under air exhibit longer-lived signals for the reaction intermediates. To extract the rate constants for the reaction steps, a kinetic model was created based on the productive and nonproductive pathways of the proposed mechanism (Supporting Information).

Initially, we focused on samples containing only $[Ru(bpz)_3]^{2+}$ and anethole under an inert atmosphere (Figure 3). This allowed us to determine the rate constants for the pathways involved in the formation of the [2 + 2] product. These pathways included the back electron transfer (BET) between Ru(I) and anethole$^{\bullet+}$ (k_{BET}), the dimerization of anethole ($k_{[2+2]}$), and the reduction of $[2 + 2]^{\bullet+}$ ($k_{red1[2+2]}$) by Ru(I). Fits of single-wavelength traces determined the value of k_{BET} to be 1.3 ($\pm$0.1) $\times 10^{10}$ M^{-1} s^{-1}, $k_{[2+2]}$ to be 5.0 ($\pm$3.0) $\times 10^7$ M^{-1} s^{-1}, and $k_{red1[2+2]}$ to be 2.9 ($\pm$0.4) $\times 10^8$ M^{-1} s^{-1}. The rate constants for these steps were in agreement with previously reported rate constants for similar single electron transfers between photocatalysts and substrates.[31,33] Specifically, Nocera and Nicewicz found rate constants for back electron transfer pathways in photoredox hydroamidation and Anti-Markovnikov hydroamination reactions to be 7.4×10^9 and 8.1×10^9 M^{-1} s^{-1}, respectively.[31,33]

With an initial set of rate constants established, we repeated the experiment with $[Ru(bpz)_3]^{2+}$ and anethole but exposed to air, which allowed us to characterize the reduction of oxygen (k_{redO2}) leading to the formation of the superoxide, reduction of the anethole radical cation by superoxide (k_{BET2}) and the reduction of $[2 + 2]^{\bullet+}$ by O_2 ($k_{red2[2+2]}$) (Figure 3). By integrating the rate constants determined under an inert atmosphere into the kinetic model for the reaction conducted open to air, we could minimize the number of unknown variables. Fits of the single-wavelength traces found the rate constants for k_{redO2} to be 3.0×10^9 M^{-1} s^{-1}, k_{BET2} to be 6.4 ($\pm$0.2) $\times 10^8$ M^{-1} s^{-1}, and $k_{red2[2+2]}$ to be 1.0 ($\pm$0.3) $\times 10^8$ M^{-1} s^{-1}.

In a similar manner, rate constants for pathways producing the [4 + 2] product were also determined using TAS. Rate constants determined for the [2 + 2] pathways were used in subsequent fits to minimize the number of new variables being considered during the fitting process. The conditions for these single-wavelength traces were identical to the [2 + 2] samples but also included 10 equiv of isoprene. Single-wavelength traces were collected under both an inert atmosphere and when exposed to air (Figure 4). Under inert conditions, the rate constants for the cyclization of anethole and isoprene ($k_{[4+2]}$) and the reduction of $[4 + 2]^{\bullet+}$ by Ru(I) ($k_{red1[4+2]}$) were found to be 1.6 ($\pm$0.4) $\times 10^8$ $M^{-1}s^{-}$ and 6.0 ($\pm$2.0) $\times 10^9$ M^{-1} s^{-1}, respectively. Previous mechanistic studies performed on cyclization reactions, such as the dimerization of benzene, found the rate constant of the cyclization pathway to be between 7.0×10^8 M^{-1} s^{-1} and 4.6 ($\pm$1.2) $\times 10^9$ M^{-1} s^{-1}.[45,46] This suggests that the rate constant found for the [4 + 2] cyclization pathway is within reason. Studies on similar photocatalytic systems involving electron transfers with metal-centered photocatalysts reducing a substrate intermediate found rate constants ranging from 8.1×10^9 to 2.1×10^{10} M^{-1} s^{-1}, which are consistent with the rate constants found for the reduction of $[4 + 2]^{\bullet+}$ by the Ru(I) intermediate.[31]

Lastly, the samples for the [4 + 2] reaction were prepared open to air. Experiments with these samples explored the

https://doi.org/10.1021/jacs.4c14255
J. Am. Chem. Soc. 2024, 146, 34900–34908

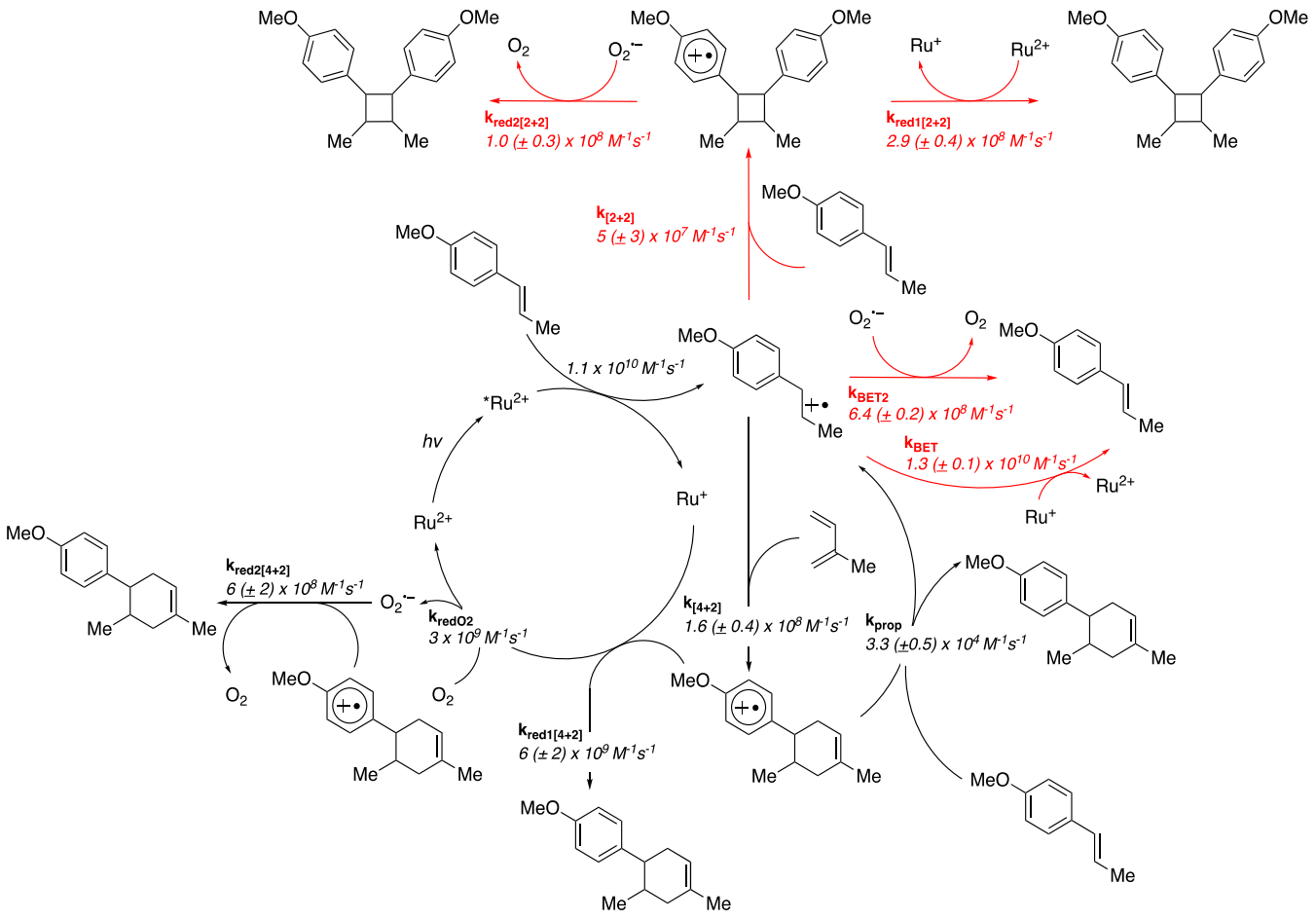

Figure 5. Overall reaction mechanism with rate constants determined via TAS and emission quenching experiments for the photoredox-catalyzed Diels−Alder reaction of *trans*-anethole and isoprene. Steps detailed with red arrows indicate unproductive pathways.

reduction of $[4 + 2]^{\bullet+}$ by oxygen ($k_{red2[4+2]}$) and the propagation step (k_{prop}), which were determined to be 6.0 (±2.0) × 10^8 M^{-1} s^{-1} and 3.3 (±0.5) × 10^4 M^{-1} s^{-1}, respectively. A previous study determined propagation rate constants for the polymerization reactions of isoprene and trimethylaminoethyl acrylate (3.1 (±0.8) × 10^5 M^{-1} s^{-1} and 6.8 (±2.0) × 10^4 M^{-1} s^{-1}, respectively)[28,47] suggesting that the value we determined is reasonable.

The rate constants found for the pathways that oxidize the Ru(I) intermediate, including k_{redO2}, $k_{red1[4+2]}$, and $k_{red1[2+2]}$, suggest that O_2 notably contributes to the success of the reaction by acting as a secondary electron acceptor. In the reaction, the concentration of O_2 is much higher than the concentrations of $[4 + 2]^{\bullet+}$ and $[2 + 2]^{\bullet+}$, which biases electron transfer from Ru(I) to O_2 instead of a radical cation species, despite the value of $k_{red1[4+2]}$ being larger than k_{redO2}. The reduction of O_2 instead of $[4 + 2]^{\bullet+}$ leaves more $[4 + 2]^{\bullet+}$ intermediate available to proceed down the propagation pathway.

Kinetic Model of the Reaction. Data from the single-wavelength traces provided kinetic information for the reaction mechanism for both productive and nonproductive pathways (Figure 5). Comparison of rate constants led to a clearer view of how the reaction functions. For example, the bulk reaction is more selective for the [4 + 2] product with 10 equiv of isoprene instead of 3 equiv, and the comparison between $k_{[2+2]}$ and $k_{[4+2]}$ demonstrates why. Both the [2 + 2] and [4 + 2] pathways go through a common anethole radical cation intermediate, with the selectivity for the [4 + 2] product controlled by the rate of each pathway. The rate constant for the [2 + 2] cyclization is approximately half the value of the [4 + 2] cyclization rate constant (5.0 (±3.0) × 10^7 M^{-1} s^{-1} vs 1.6 (±0.4) × 10^8 M^{-1} s^{-1}), so at 1 equiv of isoprene the rate for the [4 + 2] cyclization will only be 3.2 times faster. This results in the majority of the [4 + 2] product and also a significant concentration of the [2 + 2] product. Based on the rate constants for each cyclization pathway, a back of the envelope calculation would predict a yield of 10% [2 + 2] product at 3 equiv of isoprene. This is remarkably close to the [2 + 2] product yield we observe experimentally under those conditions (14.1%). Thus, for the [4 + 2] cyclization to efficiently outcompete the [2 + 2] cyclization, a higher concentration of isoprene is needed to efficiently trap the anethole radical cation before it can cyclize with another molecule of anethole. Upon increasing to 10 equiv of isoprene, we observe only a 3.6% yield of the [2 + 2] product.

The TAS data also provide valuable insights into the kinetics controlling propagation (i.e., chain behavior) versus closed cycle reactivity. We observed that the rate constant for the reduction of $[4 + 2]^{\bullet+}$ to the [4 + 2] product, $k_{red1[4+2]}$, was 5 orders of magnitude larger than the rate constant for the propagation step (k_{prop}): 6.0 (±2.0) × 10^9 M^{-1} s^{-1} and 3.3 (±0.5) × 10^4 M^{-1} s^{-1}, respectively. On the surface, this suggests that the propagation step is not a kinetically favored pathway. As above, propagation becomes competitive due to concentration effects. The propagation step is a bimolecular

https://doi.org/10.1021/jacs.4c14255
J. Am. Chem. Soc. 2024, 146, 34900−34908

reaction between $[4 + 2]^{\bullet+}$ and neutral anethole, which is at millimolar concentrations. Conversely, the reduction of $[4 + 2]^{\bullet+}$ by Ru(I) relies on two species that are in low concentration (<1 μM) at steady state. Thus, the absolute rate of the propagation pathway is competitive with the absolute rate of the closed cycle pathway, which is why we observe some chain behavior under an inert atmosphere. In the presence of oxygen, the TAS data demonstrates that electron transfer from Ru(I) to oxygen is efficient and complete within about 1 μs. The rate constant for the reduction of $[4 + 2]^{\bullet+}$ by superoxide, $k_{red2[4+2]}$, is an order of magnitude smaller than the reduction of $[4 + 2]^{\bullet+}$ by Ru(I). This makes the absolute rate of $[4 + 2]^{\bullet+}$ reduction by superoxide slower, and thus, the propagation step is better able to outcompete the closed cycle pathway. Overall, this leads to an increase in the number of chain propagation steps and QY.

To gain further insights into the performance of the reaction, kinetic modeling was implemented by using the rate constants from the TAS experiments to predict the QY of the reaction. Under air, the kinetic model was able to reasonably predict the reaction QY of the [4 + 2] reaction (Figure 6), capturing both

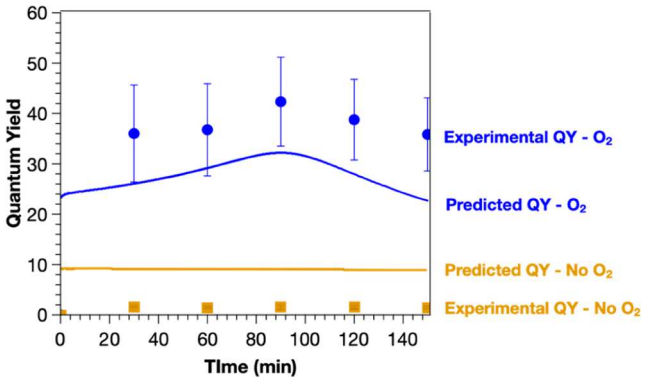

Figure 6. Experimental quantum yields for [4 + 2] photoredox cyclization under an inert atmosphere (orange square) and in air (blue circle). Solid lines are predicted quantum yields from kinetic modeling using rate constants determined from transient absorption experiments.

the magnitude of the QY as well as a peak in the QY around 90 min. Without oxygen present, the kinetic modeling predicts a substantially lower QY and is in reasonably good agreement with the experiment, although it does overestimate the QY by a factor of 2−3. This could suggest an additional pathway that we have failed to characterize. On balance, however, the kinetic modeling largely captures the key features of the QY under both inert and air atmospheres.

The kinetic modeling also enables us to assess alternative pathways in the mechanism. Recently, Moore and co-workers explored the [2 + 2] photoredox cycloaddition of anethole and made a strong argument for energy transfer from the excited photosensitizer to oxygen, leading to the formation of singlet oxygen.[43] The singlet oxygen was then proposed to undergo electron transfer from Ru(I) to form superoxide. A variety of experiments unambiguously demonstrated the presence of singlet oxygen in the reaction. Using the mechanism that Moore and co-workers proposed, we refitted our TAS data (Supporting Information) and observed that most of the rate constants were unaffected. We were also able to use kinetic modeling to explore this mechanism, and we observed that oxygen is predicted to have no effect on the reaction. We hypothesize that singlet oxygen is unable to build up in sufficient quantities to enable efficient electron transfer from Ru(I), in part because the reported lifetime of singlet oxygen in DCM is 70−90 μs and in part because the reduced photocatalyst is likely to undergo more rapid electron transfer to the more oxidizing $[4 + 2]^{\bullet+}$ than singlet oxygen.[48] Instead, we suggest that underpotential electron transfer to form singlet oxygen directly is more consistent with how the reaction performs.[49−51] It should be noted, however, that Moore and co-workers used a different photocatalyst, tris(2,2′-bipyrimidine)ruthenium(II) and were focused on the [2 + 2] cyclization reaction. The quenching rate constant of the tris(2,2′-bipyrimidine)ruthenium(II) excited state by the anethole is much lower than k_q for $[Ru(bpz)_3]^{2+}$. This suggests that energy transfer with tris(2,2′-bipyrimidine)ruthenium(II) to oxygen may be more favored than that with $[Ru(bpz)_3]^{2+}$. It is also possible that the singlet oxygen pathway plays a larger role in the [4 + 2] reaction than we propose, but unfortunately, we are unable to directly probe the oxygen intermediates and thus cannot resolve the impact of a singlet oxygen pathway.

Another advantage of using kinetic modeling is that the effect of changing rates can be easily observed in the simulation. Changing most of the rate constants in the reaction had minimal impact on the QY; however, variation of k_{prop} had a significant effect. Figure S26 shows how the predicted QY changes with k_{prop}. Below 3×10^4 M^{-1} s^{-1}, there is a significant decrease in the QY. Even with k_{prop} at 1×10^4 M^{-1} s^{-1}, the QY decreases by about 30%. Interestingly, however, with k_{prop} equal to 10^5 and 10^6 M^{-1} s^{-1}, initially, there is not a substantial difference in QY. Over the course of 60 min, however, the QY increases exponentially. This is likely due to the compounding effect of longer chain propagations with higher values of k_{prop}.

Finally, the kinetic modeling also demonstrates a clear dependence between the light intensity and the QY. We have previously demonstrated that QY in a closed cycle reaction does not depend on light intensity,[14] at least within a range of light intensities practical in a lab or commercial setting. Alternatively, kinetic modeling predicts a notable decrease in the QY of the reaction, even changing from 100 μW to 1.5 mW, with the QY predicted to further decrease with increasing light intensity (Figure S27). We hypothesize that this is related to an increase in Ru(I) at steady-state conditions and thus an increased probability of reducing $[4 + 2]^{\bullet+}$. On the basis of this, we suggest that light-dependent QY measurements may be a better strategy for identifying chain reactions than looking for a QY greater than 1 or chopped illumination, two methods generally used to identify photoredox chain reactions.[1] It should also be noted that Pitre and co-workers recently proposed a new approach for intermittent illumination of photoredox chain reactions to determine the chain propagation time.[30]

CONCLUSIONS

The intentional design of photoredox chain reactions is essential for the development of efficient and scalable photocatalysis. Understanding the kinetic and mechanistic factors that control chain propagation versus termination is necessary for the design of chain reactions. This study demonstrates the critical role that a secondary electron acceptor can play in promoting chain propagation in photochemical reactions. Specifically, we demonstrate that the key kinetic competition is between the propagation step

https://doi.org/10.1021/jacs.4c14255
J. Am. Chem. Soc. 2024, 146, 34900−34908

and the reduction of $[4 + 2]^{\bullet+}$ by the reduced photocatalyst. Electron transfer from the reduced photocatalyst to oxygen to form superoxide leads to an order of magnitude decrease in the reduction rate constant for $[4 + 2]^{\bullet+}$.

Moving forward, the selection and design of secondary electron acceptors should be a point of emphasis for the development of photoredox chain reactions. While oxygen is abundant and simple to use, reduction to superoxide or energy transfer to generate singlet oxygen results in the formation of reactive oxygen species.[50,51] The presence of ROS could introduce undesired side reactions into many reactions. Instead, future work should focus on systems that incorporate secondary electron acceptors with slow rates of electron transfer to the product radical cations.[52]

A second point of emphasis involves a better understanding of the factors that control k_{prop}. Alabugin and co-workers have done an excellent job highlighting the fundamental theory necessary for electron upconversion chain reactions;[25,53] however, gaps in our understanding still remain. Specifically, we have a poor understanding of the relationship between the rate of electron transfer and the oxidation potentials of the substrate and product radical ion. More broadly, this work demonstrates that despite 5 orders of magnitude difference between k_{prop} and $k_{red1[4+2]}$, chain reactivity was still able to occur, albeit with limited productivity in the absence of oxygen. Characterization of other photoredox chain systems is necessary to understand if this difference in rate constants between the chain-terminating and propagation steps is generally tolerated.

■ ASSOCIATED CONTENT

Supporting Information

The Supporting Information is available free of charge at https://pubs.acs.org/doi/10.1021/jacs.4c14255.

> Detailed procedure for obtaining single-wavelength traces and fitting, kinetic modeling, and QY prediction; NMR data of the synthesized ruthenium catalyst and final reaction [2 + 2] and [4 + 2] products; spectroelectrochemical difference spectra; spectra of $[2 + 2]^{\bullet+}$, $[4 + 2]^{\bullet+}$; Stern Volmer quenching of $[Ru(bpz)_3]^{2+}$; reaction QY under varying light conditions; and procedure for obtaining the lifetime of the $[Ru(bpz)_3]^{2+}$ catalyst (PDF)

■ AUTHOR INFORMATION

Corresponding Author

John R. Swierk − *Department of Chemistry, Binghamton University, Binghamton, New York 13902, United States;* orcid.org/0000-0001-5811-7285; Email: jswierk@binghamton.edu

Author

Annemarie A. Lee − *Department of Chemistry, Binghamton University, Binghamton, New York 13902, United States*

Complete contact information is available at: https://pubs.acs.org/10.1021/jacs.4c14255

Author Contributions

This manuscript was written through contributions of all authors. All authors have given approval to the final version of the manuscript.

Notes

The authors declare no competing financial interest.

■ ACKNOWLEDGMENTS

This work was supported by the National Science Foundation (Award Number CHE-2047492). A.A.L. thanks Juniper Stevenson for assistance with the TAS measurements.

■ REFERENCES

(1) Cismesia, M. A.; Yoon, T. P. Characterizing chain processes in visible light photoredox catalysis. *Chem. Sci.* **2015**, *6* (10), 5426−5434.

(2) Condie, A. G.; González-Gómez, J. C.; Stephenson, C. R. J. Visible-Light Photoredox Catalysis: Aza-Henry Reactions via C−H Functionalization. *J. Am. Chem. Soc.* **2010**, *132* (5), 1464−1465.

(3) Nicewicz, D. A.; MacMillan, D. W. Merging photoredox catalysis with organocatalysis: the direct asymmetric alkylation of aldehydes. *Science* **2008**, *322* (5898), 77−80.

(4) Spielvogel, E. H.; Stevenson, B. G.; Stringer, M. J.; Hu, Y.; Fredin, L. A.; Swierk, J. R. Insights into the Mechanism of an Allylic Arylation Reaction via Photoredox-Coupled Hydrogen Atom Transfer. *J. Org. Chem.* **2022**, *87* (1), 223−230.

(5) Arias-Rotondo, D. M.; McCusker, J. K. The photophysics of photoredox catalysis: a roadmap for catalyst design. *Chem. Soc. Rev.* **2016**, *45* (21), 5803−5820.

(6) Rillema, D. P.; Allen, G.; Meyer, T. J.; Conrad, D. Redox properties of ruthenium(II) tris chelate complexes containing the ligands 2,2′-bipyrazine, 2,2′-bipyridine, and 2,2′-bipyrimidine. *Inorg. Chem.* **1983**, *22* (11), 1617−1622.

(7) Rozenel, S. S.; Azpilcueta, C. R.; Flores-Leonar, M. M.; Rebolledo-Chávez, J. P. F.; Ortiz-Frade, L.; Amador-Bedolla, C.; Martin, E. Ruthenium tris bipyridine derivatives and their photocatalytic activity in [4 + 2] cycloadditions. An experimental and DFT study. *Catal. Today* **2018**, *310*, 2−10.

(8) Teegardin, K.; Day, J. I.; Chan, J.; Weaver, J. Advances in Photocatalysis: A Microreview of Visible Light Mediated Ruthenium and Iridium Catalyzed Organic Transformations. *Org. Process Res. Dev.* **2016**, *20* (7), 1156−1163.

(9) Fukuzumi, S.; Hironaka, K.; Tanaka, T. Photoreduction of alkyl halides by an NADH model compound. An electron-transfer chain mechanism. *J. Am. Chem. Soc.* **1983**, *105* (14), 4722−4727.

(10) Lamberth, C.; Jeanmart, S.; Luksch, T.; Plant, A. Current Challenges and Trends in the Discovery of Agrochemicals. *Science* **2013**, *341* (6147), 742−746.

(11) Swierk, J. R. The Cost of Quantum Yield. *Org. Process Res. Dev.* **2023**, *27* (7), 1411−1419.

(12) Turner, M. K. Pharmaceuticals from agriculture: manufacture of discovery? *Ind. Crops Prod.* **1992**, *1* (2−4), 125−131.

(13) Braslavsky, S. E.; Braun, A. M.; Cassano, A. E.; Emeline, A. V.; Litter, M. I.; Palmisano, L.; Parmon, V. N.; Serpone, N. Glossary of terms used in photocatalysis and radiation catalysis (IUPAC Recommendations 2011). *Pure Appl. Chem.* **2011**, *83* (4), 931−1014.

(14) Stevenson, B. G.; Spielvogel, E. H.; Loiaconi, E. A.; Wambua, V. M.; Nakhamiyayev, R. V.; Swierk, J. R. Mechanistic Investigations of an α-Aminoarylation Photoredox Reaction. *J. Am. Chem. Soc.* **2021**, *143* (23), 8878−8885.

(15) Bodenstein, M. Chain Reactions. *Chem. Rev.* **1930**, *7* (2), 215−223.

(16) Crellin, R. A.; Lambert, M. C.; Ledwith, A. Photochemical 2 + 2 cycloaddition via a cation-radical chain reaction. *J. Chem. Soc. D* **1970**, No. 11, 682−683.

(17) Schutte, R.; Freeman, G. R. Radiation-induced dimerization of 1,3-cyclohexadiene. Solvent effects and the formation of the Diels-Alder dimers by a cationic chain mechanism. *J. Am. Chem. Soc.* **1969**, *91* (14), 3715−3720.

(18) Lin, S.; Ischay, M. A.; Fry, C. G.; Yoon, T. P. Radical Cation Diels−Alder Cycloadditions by Visible Light Photocatalysis. *J. Am. Chem. Soc.* **2011**, *133* (48), 19350−19353.

(19) Paulisch, T. O.; Strieth-Kalthoff, F.; Henkel, C.; Pitzer, L.; Guldi, D. M.; Glorius, F. Chain propagation determines the chemo- and regioselectivity of alkyl radical additions to C−O vs. C−C double bonds. *Chem. Sci.* **2020**, *11* (3), 731−736.
(20) Wang, Q.; Wang, Q.; Zhang, Y.; Mohamed, Y. M.; Pacheco, C.; Zheng, N.; Zare, R. N.; Chen, H. Electrocatalytic redox neutral [3 + 2] annulation of N-cyclopropylanilines and alkenes. *Chem. Sci.* **2021**, *12* (3), 969−975.
(21) Percec, V.; Guliashvili, T.; Ladislaw, J. S.; Wistrand, A.; Stjerndahl, A.; Sienkowska, M. J.; Monteiro, M. J.; Sahoo, S. Ultrafast Synthesis of Ultrahigh Molar Mass Polymers by Metal-Catalyzed Living Radical Polymerization of Acrylates, Methacrylates, and Vinyl Chloride Mediated by SET at 25 °C. *J. Am. Chem. Soc.* **2006**, *128* (43), 14156−14165.
(22) Studer, A.; Curran, D. P. Catalysis of Radical Reactions: A Radical Chemistry Perspective. *Angew. Chem., Int. Ed.* **2016**, *55* (1), 58−102.
(23) Allen, P. E. M.; Patrick, C. R. Generation of Radicals in Pairs and the Kinetics of Radical Chain Reactions in Solution. *Nature* **1961**, *191* (4794), 1194−1195.
(24) Kubota, K.; Jiang, J.; Kamakura, Y.; Hisazumi, R.; Endo, T.; Miura, D.; Kubo, S.; Maeda, S.; Ito, H. Using Mechanochemistry to Activate Commodity Plastics as Initiators for Radical Chain Reactions of Small Organic Molecules. *J. Am. Chem. Soc.* **2024**, *146* (1), 1062−1070.
(25) Chabuka, B. K.; Alabugin, I. V. Hole Catalysis of Cycloaddition Reactions: How to Activate and Control Oxidant Upconversion in Radical-Cationic Diels−Alder Reactions. *J. Am. Chem. Soc.* **2023**, *145* (35), 19354−19367.
(26) Talbott, E. D.; Burnett, N. L.; Swierk, J. R. Mechanistic and kinetic studies of visible light photoredox reactions. *Chem. Phys. Rev.* **2023**, *4* (3), No. 031312, DOI: 10.1063/5.0156850.
(27) Kandoth, N.; Pérez Hernández, J.; Palomares, E.; Lloret-Fillol, J. Mechanisms of photoredox catalysts: the role of optical spectroscopy. *Sustain. Energy Fuels* **2021**, *5* (3), 638−665.
(28) Lewis-Borrell, L.; Sneha, M.; Bhattacherjee, A.; Clark, I. P.; Orr-Ewing, A. J. Mapping the multi-step mechanism of a photoredox catalyzed atom-transfer radical polymerization reaction by direct observation of the reactive intermediates. *Chem. Sci.* **2020**, *11* (17), 4475−4481.
(29) Martinez-Haya, R.; Miranda, M. A.; Marin, M. L. Metal-Free Photocatalytic Reductive Dehalogenation Using Visible-Light: A Time-Resolved Mechanistic Study. *Eur. J. Org. Chem.* **2017**, *2017* (15), 2164−2169.
(30) Pitre, S. P.; McTiernan, C. D.; Scaiano, J. C. Understanding the Kinetics and Spectroscopy of Photoredox Catalysis and Transition-Metal-Free Alternatives. *Acc. Chem. Res.* **2016**, *49* (6), 1320−1330.
(31) Qin, Y.; Zhu, Q.; Sun, R.; Ganley, J. M.; Knowles, R. R.; Nocera, D. G. Mechanistic Investigation and Optimization of Photoredox Anti-Markovnikov Hydroamination. *J. Am. Chem. Soc.* **2021**, *143* (27), 10232−10242.
(32) Wang, C.; Malinoski, A. Perspective: Mechanistic investigations of photocatalytic processes with time-resolved optical spectroscopy. *J. Chem. Phys.* **2022**, *157* (16), No. 160901, DOI: 10.1063/5.0111162.
(33) Ruccolo, S.; Qin, Y.; Schnedermann, C.; Nocera, D. G. General Strategy for Improving the Quantum Efficiency of Photoredox Hydroamidation Catalysis. *J. Am. Chem. Soc.* **2018**, *140* (44), 14926−14937.
(34) Romero, N. A.; Nicewicz, D. A. Mechanistic Insight into the Photoredox Catalysis of Anti-Markovnikov Alkene Hydrofunctionalization Reactions. *J. Am. Chem. Soc.* **2014**, *136* (49), 17024−17035.
(35) Yayla, H. G.; Peng, F.; Mangion, I. K.; McLaughlin, M.; Campeau, L.-C.; Davies, I. W.; DiRocco, D. A.; Knowles, R. R. Discovery and mechanistic study of a photocatalytic indoline dehydrogenation for the synthesis of elbasvir. *Chem. Sci.* **2016**, *7* (3), 2066−2073.
(36) Lattke, Y. M.; Corbin, D. A.; Sartor, S. M.; McCarthy, B. G.; Miyake, G. M.; Damrauer, N. H. Interrogation of O-ATRP Activation Conducted by Singlet and Triplet Excited States of Phenoxazine Photocatalysts. *J. Phys. Chem. A* **2021**, *125* (15), 3109−3121.
(37) Cai, Y.; Wang, J.; Zhang, Y.; Li, Z.; Hu, D.; Zheng, N.; Chen, H. Detection of Fleeting Amine Radical Cations and Elucidation of Chain Processes in Visible-Light-Mediated [3 + 2] Annulation by Online Mass Spectrometric Techniques. *J. Am. Chem. Soc.* **2017**, *139* (35), 12259−12266.
(38) Koyama, D.; Dale, H. J. A.; Orr-Ewing, A. J. Ultrafast Observation of a Photoredox Reaction Mechanism: Photoinitiation in Organocatalyzed Atom-Transfer Radical Polymerization. *J. Am. Chem. Soc.* **2018**, *140* (4), 1285−1293.
(39) Lies, S. D.; Lin, S.; Yoon, T. P. Visible Light Photocatalysis of Radical Cation Diels-Alder Cycloadditions: Preparation of Tris(2,2′-bipyrazyl) Ruthenium(II) Bis(tetrakis(3,5-bis(trifluoromethyl)-phenyl)borate). *Org. Synth.* **2016**, *93* (93), 178−199.
(40) Shirono, K.; Morimatsu, T.; Takemura, F. Gas Solubilities (CO2, O2, Ar, N2, H2, and He) in Liquid Chlorinated Methanes. *J. Chem. Eng. Data* **2008**, *53* (8), 1867−1871.
(41) Demas, J. N.; Diemente, D.; Harris, E. W. Oxygen quenching of charge-transfer excited states of ruthenium(II) complexes. Evidence for singlet oxygen production. *J. Am. Chem. Soc.* **1973**, *95* (20), 6864−6865.
(42) Abdel-Shafi, A. A.; Ward, M. D.; Schmidt, R. Mechanism of quenching by oxygen of the excited states of ruthenium(ii) complexes in aqueous media. Solvent isotope effect and photosensitized generation of singlet oxygen, O2(1Δg), by [Ru(diimine)(CN)4]2− complex ions. *Dalton Trans.* **2007**, No. 24, 2517−2527.
(43) Quach, G.; Iranmanesh, H.; Luis, E. T.; Harper, J. B.; Beves, J. E.; Moore, E. G. Mechanistic and Kinetic Insights into Intermolecular [2 + 2] Photocycloadditions. *ACS Catal.* **2024**, *14* (11), 8758−8766.
(44) Bronner, C.; Wenger, O. S. Long-range proton-coupled electron transfer in phenol−Ru(2,2′-bipyrazine)32+ dyads. *Phys. Chem. Chem. Phys.* **2014**, *16* (8), 3617−3622.
(45) Porter, G.; Steinfeld, J. I. Rate of dimerisation of gaseous benzyne. *J. Chem. Soc. A* **1968**, 877−878.
(46) Schafer, M. E.; Berry, R. S. The Dimerization of Gaseous Benzyne. *J. Am. Chem. Soc.* **1965**, *87* (20), 4497−4501.
(47) Kattner, H.; Buback, M. Termination, Transfer, and Propagation Kinetics of Trimethylaminoethyl Acrylate Chloride Radical Polymerization in Aqueous Solution. *Macromolecules* **2017**, *50* (11), 4160−4168.
(48) Salokhiddinov, K. I.; Byteva, I. M.; Gurinovich, G. P. Lifetime of singlet oxygen in various solvents. *J. Appl. Spectrosc.* **1981**, *34* (5), 561−564.
(49) Winterle, J. S.; Kliger, D. S.; Hammond, G. S. Mechanisms of photochemical reactions in solution. 80. Photochemical oxidation of tris(2,2′-bipyridyl)ruthenium(II) by molecular oxygen. *J. Am. Chem. Soc.* **1976**, *98* (12), 3719−3721.
(50) Navarro, J. A.; Roncel, M.; De La Rosa, F. F.; De La Rosa, M. A. Hydrogen peroxide photoproduction by the semicarbazide—tris(2,2′-bipyridine)ruthenium(II)—oxygen system. *J. Photochem. Photobiol., A* **1987**, *40* (2), 279−293.
(51) Kalyanasundaram, K. Photophysics, photochemistry and solar energy conversion with tris(bipyridyl)ruthenium(II) and its analogues. *Coord. Chem. Rev.* **1982**, *46*, 159−244.
(52) Miyuranga, K. A. V.; Ashcraft, K.; Pitre, S. Modern Approach to Intermittent Illumination for the Characterization of Chain-Propagation in Photoredox Catalysis *ChemRxiv* 2024 DOI: 10.26434/chemrxiv-2024-vrsw4-v2.
(53) Syroeshkin, M. A.; Kuriakose, F.; Saverina, E. A.; Timofeeva, V. A.; Egorov, M. P.; Alabugin, I. V. Upconversion of Reductants. *Angew. Chem., Int. Ed.* **2019**, *58* (17), 5532−5550.